UC Irvine

UC Irvine Previously Published Works

Title

Optical Coherence Tomography Patterns in the Molecular Diagnosis and Treatment Response of Port Wine Capillary Malformations (Port Wine Birthmarks).

Permalink

https://escholarship.org/uc/item/5h19162c

Journal

Lasers Surg Med

Authors

Le, Todd
Evans, Edward L
Hetzel, Scott
et al.

Publication Date

2026-11-05

DOI

10.1002/lsm.70223

Copyright Information

This work is made available under the terms of a Creative Commons Attribution License, available at https://creativecommons.org/licenses/by/4.0/

Peer reviewed

eScholarship.org Powered by the California Digital Library
University of California

Check for updates

Lasers in Surgery and Medicine

CLINICAL ARTICLE OPEN ACCESS

Optical Coherence Tomography Patterns in the Molecular Diagnosis and Treatment Response of Port Wine Capillary Malformations (Port Wine Birthmarks)

Todd Le[1] | Edward L. Evans III[2] | Scott Hetzel[3] | Feben Messele[4] | Rachel Elsanadi[4] | Allison Miller[1] | Olamide Sonuga[4] | Ashley Ng[1] | John Moon[1] | Jennifer Tran[1] | Ellen Bruhn[1] | Walter Block[5] | Kevin W. Eliceiri[2,3,5] | Beth Drolet[1] | Kristen M. Kelly[4] | Lisa Arkin[1]

[1]Department of Dermatology, University of Wisconsin, Madison, Wisconsin, USA | [2]Center for Quantitative Cell Imaging, University of Wisconsin-Madison, Madison, Wisconsin, USA | [3]Department of Biostatistics and Medical Informatics, University of Wisconsin, Madison, Wisconsin, USA | [4]Department of Dermatology, University of California-Irvine, Irvine, California, USA | [5]Department of Biomedical Engineering, University of Wisconsin, Madison, Wisconsin, USA

Correspondence: Lisa Arkin (larkin@dermatology.wisc.edu)

Received: 25 June 2026 | **Revised:** 9 September 2026 | **Accepted:** 19 October 2026

Funding: Sturge-Weber Foundation; Dermatology Foundation, Grant/Award Number: Arkin CDA 2020; Pediatric Dermatology Research Alliance; NIH P41 GM135019, Grant/Award Number: UW ICTR and Skin Disease Research Center

Keywords: capillary malformation | *EPHB4* | *GNAQ* | optical coherence tomography | port-wine birthmark | pulsed dye laser | *RASA1* | Sturge-Weber Syndrome

ABSTRACT

Objectives: To evaluate whether dynamic optical coherence tomography (D-OCT) vascular characteristics correlate with molecular diagnosis or laser treatment response in port wine capillary malformations.

Methods: D-OCT imaging was performed in a cross-sectional prospective of patients with clinically confirmed port wine capillary malformations. Vessel diameter was assessed using proprietary software and watershed segmentation and compared by genotype, clinical features, and treatment response.

Results: 47 subjects were recruited, with 173 D-OCT images which were captured without artifact and met inclusion criterion. Quantitative vascular measurements did not differ significantly between low-flow (GNAQ/GNA11) and fast-flow (EPHB4/RASA1) lesions. In contrast, vessel diameters were significantly greater with laser-resistant lesions after adjustment for confounders ($p < 0.001$).

Conclusions: D-OCT did not show significant genotype discrimination in this cohort but might offer a potential noninvasive biomarker for predicting laser treatment outcomes. Further prospective studies with greater power are required to validate these findings and to determine the clinical relevance for laser treatment parameters in affected patients.

1 | Introduction

Port wine capillary malformations (PWCMs) represent a diagnostic grouping of genetically diverse vascular anomalies which present at birth as light pink to purple vascular patches on the skin and progressively darken with time. Nearly all PWCMs are caused by mosaic activating variants in genes that regulate cell growth, vascular homeostasis, and fetal vasculature development. The International Society for the Study of Vascular Anomalies (ISSVA) has defined PWCM as a group that includes "low-flow" lesions, which produce classic block-like, segmental PWCM, and "fast-flow" lesions, which produce capillary malformations overlying and at risk for high flow arteriovenous

This is an open access article under the terms of the Creative Commons Attribution License, which permits use, distribution and reproduction in any medium, provided the original work is properly cited.

© 2026 The Author(s). *Lasers in Surgery and Medicine* published by Wiley Periodicals LLC.

shunting [1–5], Within the updated 2025 ISSVA classification for vascular anomalies, low-flow and fast-flow phenotypes are categorized separately as they represent mechanistically distinct pathophysiology's which diverge at the level of the driver pathway. Activating variants in the genes GNAQ/GNA11 are most common in low-flow PWCMs and underlie classic port wine birthmarks, but PIK3CA, PIK3R1, and other variants have been reported [2–4, 6]. Fast-flow PWCMs are characterized by germline loss of function and mosaic activating variants in EPHB4 and RASA1; phenotypically, these look more variegated and telangiectatic with surrounding vascular steal, and are a hallmark finding of the Capillary Malformation-Arteriovenous Malformation Syndrome (CM-AVM Syndrome) [7, 8]. Surveillance differs considerably based on molecular diagnosis: patients with EBPHB4/RASA1 variants are at risk for arteriovenous malformations involving the brain/spine and require serial CNS imaging, while those with GNAQ and GNA11 variants involving the forehead are at risk for ocular and/or brain involvement, and require serial ophthalmologic and neurologic evaluation [9, 10]. Most PWCMs harbor affected variants at very low allele frequency, in $<10\%$–15% of cells within a 4 mm biopsy, but some variants may be fatal in utero at higher variant allele frequencies [11, 12]. Currently, somatic genetic testing requires next-generation sequencing (NGS) of affected skin, which leaves a scar [11, 13].

Independent of their genetic underpinnings, PWCMs are recognized as slowly progressive. The standard of care treatment is laser via the principle of selective photothermolysis to target the proliferative vasculature, sparing surrounding tissue [14]. In up to 50% of untreated adults with low-flow PWCMs on the face, the development of progressive nodularity, vascular blebs, and soft tissue overgrowth leads to stigmatizing disfigurement by age 50, significantly reducing quality of life [15, 16]. Parallel to their phenotypic heterogeneity, the response to laser treatment of PWCMs is remarkably variable, with some patients demonstrating impressive treatment response, while others fail to improve [17–20]. A variety of intrinsic factors have been reported to influence laser treatment response, including patient age at initiation of treatment, skin thickness based on location, vessel size, and depth of the aberrant vasculature [17, 18, 20].

Dynamic optical coherence tomography angiography (D-OCT) is a noninvasive, skin-specific validated imaging modality that utilizes speckle variance to detect blood flow, generating high-resolution, depth-resolved volumetric images of the cutaneous vasculature [21]. D-OCT can visualize vessels to a depth of approximately 2 mm, but its sensitivity for detecting blood flow and vessel morphology is highest in the superficial dermis (typically up to 0.5 mm), with reduced sensitivity at greater depths due to optical scattering and signal attenuation [22, 23]. The technique is rapid, requiring about 30 s of patient stillness to acquire non-invasive images and quantitative parameters of the cutaneous vasculature for a 6×6 mm area [23]. Recent studies have investigated whether D-OCT-derived parameters—modal vessel diameter, vascular density, and depth of the vasculature—can inform more precise, individualized laser treatment strategies for PWCM. These vessel characteristics have not shown a consistent or clear correlation with lesional color, and significant heterogeneity exists, both between and within the same CM [24–27]. This heterogeneity might contribute to variable responses to laser therapy and highlights the need for further research to establish relevant imaging biomarkers for treatment planning.

The aim of this study was to determine whether D-OCT could be used to discriminate changes in the underlying PWCM vasculature, including differences based on genotype, patient age, birthmark location, and treatment response to laser. The study was cross-sectional, with at least two images generated from each subject's birthmark compared to anatomically matched non-affected control skin. We used raw images generated and assessed by the D-OCT device's proprietary algorithm and compared them to open-source watershed segmentation analysis.

2 | Methods

2.1 | Subject Recruitment

Patients with block-like, segmental or round pink, purple, or red vascular patches and a clinical diagnosis of “low-flow” or “fast-flow” PWCM were recruited from two sites: the University of Wisconsin-Madison, and University of California-Irvine. IRB approval was obtained independently from each site, and written consent was obtained from each patient and/or parent. Subject baseline demographics and clinical characteristics, including age, gender, PWCM location, and previous laser treatments (number and age at initiation), were extracted from the medical records. At least two OCT images were captured from the same birthmark in each patient, but some patients had more images captured based on the age, size, and location of the PWCM, as young children were less likely to sit still for the duration of the capture. Across all subject encounters, the environmental conditions of the room were kept as consistent as possible, including room temperature and the positioning of the patient. After photographic review by the principal investigators (LA/KK), those undergoing laser treatment were stratified by treatment response relative to baseline photographs. At each OCT imaged site, subjects with $\geq 70\%$ clearance were deemed “laser responsive” and those with $<70\%$ clearance were deemed “laser resistant.” Consensus agreement was reached by the investigators in discrepant cases. At the time of enrollment, patients could consent to a 4-mm punch biopsy of the CM for next-generation sequencing (NGS) for molecular diagnosis. After informed consent, subjects received imaging of affected and contralateral anatomically matched control skin scanned by the VivoSight Dx (Michelson Diagnostics Ltd, Kent, England) device.

2.2 | Next-Generation Sequencing

Targeted NGS using a hybrid capture approach was performed on DNA samples from affected tissues. The sequencing panel (Washington University Pathology Services Mosaicism Disorders Testing) is enriched for 177 genes associated with cancer and designed to be highly sensitive with $>1000\times$ unique, on-target reads across the capture space. A sensitive variant-calling pipeline includes capture of variants down to an allele frequency of 1.5%. Alignment to the reference genome was performed using Novoalign 3.02.06 (Novocraft Technologies,

10969101, 0, Downloaded from https://onlinelibrary.wiley.com/doi/10.1002/lsm.70223 by University Of California Irvine Science Library Serials, Wiley Online Library on [06/11/2026]. See the Terms and Conditions (https://onlinelibrary.wiley.com/terms-and-conditions) on Wiley Online Library for rules of use; OA articles are governed by the applicable Creative Commons License

Selangor, Malaysia). Lines of evidence supporting pathogenicity were extrapolated from best practices in the setting of constitutional and mosaic disease. Based on the 2025 ISSVA classification, subjects with confirmed variants in GNAQ and GNA11, the most common PWCM variants, were classified as "low-flow," while RASA1/EPHB4 variants (germline and/or mosaic) associated with CV-AVM Syndrome were classified as "fast-flow." In this cohort, other variants reported in PWCMs were not detected.

2.3 | OCT Imaging and Algorithmic Analysis

At enrollment and/or prior to laser therapy for clinical care, D-OCT was performed, with multiple images generated from the same birthmark in different locations. The Vivosight Dx has a field of view of 6×6 mm with a resolution of < 5 μm axially and < 7.5 μm laterally. Vascular images from multiple different areas on each patient were generated for review. From each image, median vessel diameter and density at the superficial vascular plexus (defined by the half-way point between the skin surface and the depth at which blood flow is highest) were calculated by incorporated proprietary software algorithms of the D-OCT system. Movement of the patient during D-OCT creates motion artifact signals. Any scan with > 50% artifact was not analyzed; these patients were excluded from analysis.

2.4 | D-OCT Vascular Network Analysis via Watershed Algorithm (Fiji)

As a second means of analysis, and to account for non-uniformity of blood vessel network orientations, watershed segmentation analysis was also pursued to approximate the mean vessel diameter. D-OCT scans were binarized through global thresholding in MATLAB (Natick, Massachusetts, USA) to isolate the vasculature from the background (Figure S1). Next, using Fiji, the watershed segmentation operation was applied to binary images to process the vasculature into discrete segments, whose diameters could be approximated [28]. The watershed segmentation function works by creating a Euclidean Distance Map (EDM), the distance of each pixel to its nearest background pixel, and then finds the Ultimate Eroded Points (UEP), the maxima of the EDM. Together, the EDM and UEP are used in the watershed segmentation algorithm to split objects at the area of narrowing blood vessels. This allows for surrogate or approximate measurement of vascular diameter within each image, despite a non-uniform network orientation. The median of all measured vessel areas was compared to the vessel diameter data generated from the D-OCT algorithm.

2.5 | Statistical Analysis

Univariable and multivariable mixed effects ANOVA models were fit to compare the measurements of both the proprietary algorithm (D-OCT) and watershed analysis, separately, between demographic and PWCM characteristic variables of interest. Multivariable mixed effects controlled for subject age, age at ever-initiation of laser, and the number of previous laser treatments. Per subject, PWCM and anatomically matched control skin were given a unique pair ID; this was used as the random effect of the mixed effects ANOVA model. Post-hoc analyses with Tukey adjustment were examined in cases of a significant ANOVA F-test p-value. To examine the linear relationship between D-OCT and watershed measurements, R^2 was calculated via a mixed-effects linear regression model. All analyses were conducted using R for statistical computing version 4.1 with a 5% significance level for all tests. The reported p-values are from multivariable analysis tests unless otherwise noted.

3 | Results

3.1 | Patient Population

Among the 47 subjects recruited for the study, 16 were excluded due to images with > 50% motion artifact, or, less commonly, absence of clinical photos to assess treatment response. Of the remaining 31 subjects (13 male, 18 female) ages 4 weeks to 66 years, a total of 173 D-OCT scans were available for proprietary algorithm analysis and 212 were available for watershed analysis (Table 1). One subject lacked OCT algorithm data and was analyzed solely via watershed analysis. Among those subjects who consented to NGS, 12 were found to have genotypes associated with "low-flow" PWCM (10 GNAQ, 2 GNA11), and 4 patients were found to have genotypes associated with "fast-flow" PWCM (3 RASA1, 1 EPHB4). PIK3CA and other previously reported variants were not detected in the cohort evaluated. The variant allele frequency, which reports the percentage of affected mutated cells in a 4 mm punch biopsy was < 5% in all subjects, (GNAQ 2.2%–4.7%) and GNA11 (1.2%–3.5%). Among the 16 patients with confirmed genotyping, there was alignment between genotype and phenotype based on the existing vascular anomalies literature [1–5]. Those with GNAQ/GNA11 variants presented with block-like/segmental purple to pink vascular patches, with blebs and overgrowth in older subjects naïve to treatment and a diagnosis of Sturge Weber Syndrome in those with extensive forehead involvement. Those with RASA1/EPHB4 variants presented with variegated telangiectatic pink to purple patches with surrounding vascular steal. See Table S1 for further details.

The remaining 16 subjects either did not consent to genetic testing ($n = 12$) due to concern for scarring in a facial location, or had NGS performed, which failed to reveal a pathogenic variant ($n = 4$). Subjects who lacked confirmatory genotyping were not classified as "low-flow" or "fast-flow," but their images were analyzed for treatment responsiveness. Across all subjects, 15/31 (48%) were imaged with OCT prior to any treatment with laser. 15/31 (~48%) were deemed "laser responsive" at all OCT-imaged sites (indicating a global treatment response within the birthmark), while 10/31(32%) were deemed "laser resistant" at all OCT-imaged sites (indicating a poor global response within the birthmark). Those patients deemed "laser resistant" had PWCM on the medial/lateral cheek, mandible, temple, and nasal sidewall. Two out of 31 patients (~6%) had at least 1 OCT-imaged site within their birthmark, which was deemed "laser resistant" and at least 1 OCT-imaged site deemed "laser responsive," suggesting variability within the PWCM in terms of treatment response. 4 patients were untreated with laser throughout the course of the study. The median number of laser treatments across the cohort was 7.5 (range 0–30). Full case details of the series are available in Table S1.

10969101, 0, Downloaded from https://onlinelibrary.wiley.com/doi/10.1002/lsm.70223 by University Of California Irvine Science Library Serials, Wiley Online Library on [06/11/2026]. See the Terms and Conditions (https://onlinelibrary.wiley.com/terms-and-conditions) on Wiley Online Library for rules of use; OA articles are governed by the applicable Creative Commons License

TABLE 1 | Demographics of the cohort.

		D-OCT Analysis		Watershed analysis	
		Patients ($n = 31$)	**Scans ($n = 173$)**	**Patients ($n = 32$)**	**Scans ($n = 212$)**
Gender	Male	14 (45.2%)	87 (50.3%)	14 (43.8%)	86 (40.6%)
	Female	17 (54.8%)	86 (49.7%)	18 (56.3%)	126 (59.4%)
Age	Years (median [range])		12.0 (0.1– 66.0)		19.0 (0.1–66.0)
	< 2 years	4 (12.9%)	38 (22.0%)	4 (12.5%)	38 (17.9%)
	2–18 years	17 (54.8%)	68 (39.3%)	17 (53.1%)	68 (32.1%)
	19–39 years	5 (16.1%)	30 (17.3%)	5 (15.6%)	30 (14.2%)
	40+ years	5 (16.1%)	37 (21.4%)	6 (18.8%)	76 (35.8%)
Genotype	Low-flow (GNAQ)	10 (32.3%)	69 (39.9%)	11 (34.4%)	106 (50.0%)
	Low-flow (GNA11)	2 (6.5%)	3 (1.7%)	2 (6.3%)	3 (1.4%)
	High-flow (EPBH4)	1 (3.2%)	4 (2.3%)	1 (3.1%)	4 (1.9%)
	High-flow (RASA1)	3 (9.7%)	5 (2.9%)	3 (9.4%)	5 (2.4%)
	Unknown/Untested	15 (48.4%)	48 (27.7%)	15 (46.9%)	48 (22.6%)
	Control	31 (100%)	44 (25.4%)	32 (100%)	46 (21.7%)
Lesion location	Head/Neck	26 (83.9%)	153 (88.4%)	27 (84.4%)	190 (89.6%)
	Trunk	3 (9.7%)	8 (4.6%)	3 (9.4%)	8 (3.8%)
	Limbs	4 (12.9%)	12 (6.9%)	5 (15.6%)	14 (6.6%)
Treatment status	Control	31 (100%)	44 (25.4%)	32 (100%)	46 (21.7%)
	Untreated	4 (13%)	27 (15.6%)	4 (13.3%)	27 (12.7%)
	Clinically responsive*	18 (58.1%)	65 (37.6%)	18 (56.3%)	65 (30.7%)
	Clinically resistant*	13 (41.9%)	37 (21.4%)	14 (43.8%)	74 (34.9%)
	Clinically responsive/ resistant at differing locations	2/ 31 (6.5%)			

Note: Variables that are PWCM specific may have a cumulative percentage > 100% in the patient column due to patients having multiple PWCM that could cover multiple designations within a specific variable.
*Responsiveness is based on ≥ 70% clearance.

3.2 | Qualitative Trends in D-OCT Images

First, qualitative trends in the D-OCT images were analyzed alongside clinical images. Side-by-side comparison of D-OCT scans of "low-flow" (GNA-variant PWCMs) and "fast-flow" (EPHB4/RASA1 PWCMs) revealed qualitatively different imaging patterns, with significant heterogeneity in vessel diameter by genotype compared to anatomically matched control skin (Figures 1 and S2). Through this qualitative review, mosaic GNA variants demonstrated areas with larger, distorted vessels compared to dense, more narrow vessels in those with RASA1 and EPHB4 variants. OCT images from anatomically matched control skin were distinct from images of CM and qualitatively similar across all control areas. However, there was significant heterogeneity between the "low-flow" GNA variant images, with some normal appearing vessels, in contrast to the larger, architecturally distorted vessels (Figure 1).

3.3 | D-OCT Vascular Network Analysis via Device Algorithm

Following this qualitative evaluation, quantitative metrics were generated for statistical analysis (Table 2). First, modal vessel diameters were measured by the proprietary algorithm of the D-OCT device and then anatomically matched control skin. Statistically significant differences were not observed between "low-flow" and "fast-flow" genotypes (EPHB4/RASA1 vs. GNAQ/GNA11) ($p = 0.742$). Statistically significant differences in vessel diameter were noted between "low-flow" (GNA variant PWCMs) and control skin ($p < 0.001$), but not when comparing vessel diameters of "fast-flow" variants (EPHB4 and RASA1) and control skin ($p = 0.174$). Stratified by location, PWCMs in the head and neck region were of greater diameter compared to those on the extremities (*univariable* $p = 0.034$), but this was not statistically significant in the multivariable analysis ($p = 0.080$). When stratified by age (≤ 2 years, > 2 ≤ 18 years old, > 18 < 39 years old, and > 39 years), there were no significant differences in vascular diameter observed between age groups ($p = 0.515$).

After adjustment for confounders, including the number of laser treatments and age at initiation of treatment, statistically significant differences in vessel diameters were observed at OCT-sites deemed "laser responsive" (definition ≥ 70% clearance by consensus photographic review) relative to those sites deemed "laser resistant" ($p < 0.001$), with increased vessel diameters in those with poor response to treatment. Supporting this, increased vessel diameters were found in CMs "never treated with laser" ($p = 0.001$) and those deemed clinically "laser resistant" compared to anatomically matched control

10969101, 0, Downloaded from https://onlinelibrary.wiley.com/doi/10.1002/lsm.70223 by University Of California Irvine Science Library Serials, Wiley Online Library on [06/11/2026]. See the Terms and Conditions (https://onlinelibrary.wiley.com/terms-and-conditions) on Wiley Online Library for rules of use; OA articles are governed by the applicable Creative Commons License

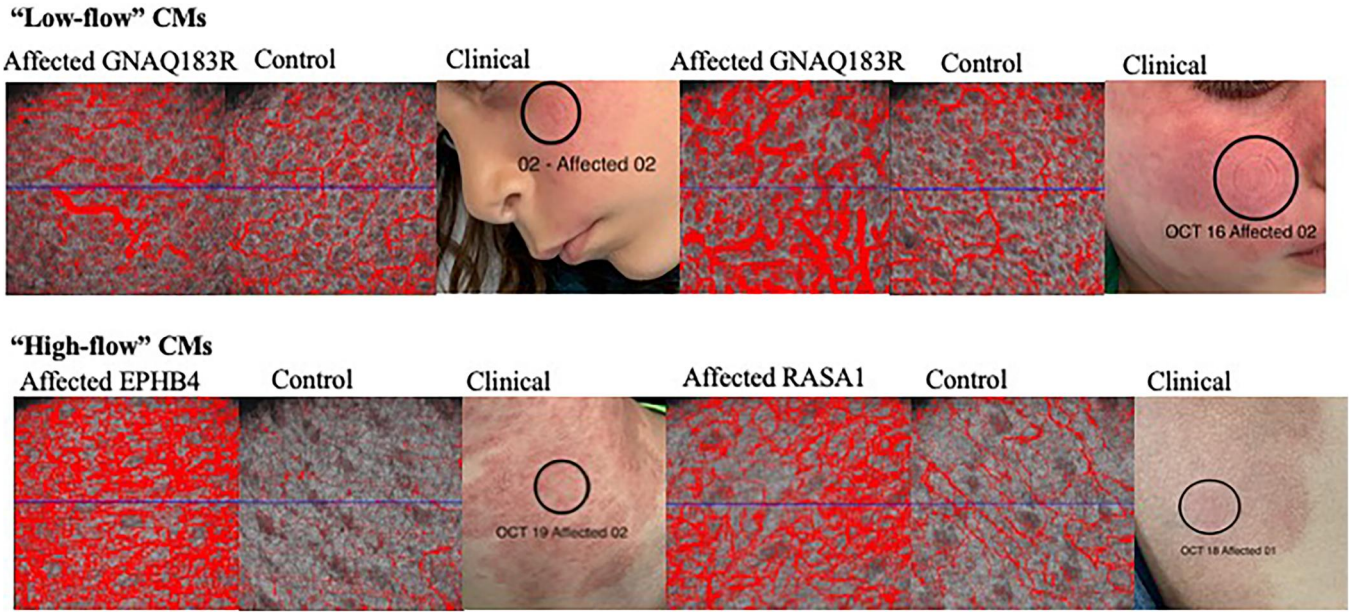

FIGURE 1 | Side-by-side representative images from D-OCT scans of vasculature of skin with confirmed (1st panel) "low flow" GNAQR183 mutations compared to anatomically matched control skin, with corresponding clinical images. In the 2nd panel, "fast flow" affected EPHB4 mutation, control skin, and clinical images are demonstrated next to affected RASA1 mutation, control skin, and clinical images. Qualitatively, differences are noted between "low-flow" and "fast-flow" variants, which were not statistically significant across the entire genotyped population.

skin ($p < 0.001$). Finally, those deemed "laser responsive" demonstrated no differences in vessel diameter compared to anatomically matched control skin ($p = 0.458$).

3.4 | D-OCT Vascular Network Analysis by Watershed Algorithm

Watershed analysis in the open-source image processing program Fiji (22) was subsequently pursued and compared to the proprietary algorithm of the D-OCT device to determine whether an alternative approximation of vessel diameters could provide additional explanatory insight. The data was statistically nonsignificant when compared to the OCT device algorithm above (Table 3). No differences were observed between genotypes using watershed analysis ($p = 0.609$). CMs on the head and neck had significantly increased vessel areas compared to CMs on extremities ($p < 0.001$). There was no difference in watershed analysis measurements of vascular networks when stratified by age ($p = 0.803$).

Finally, as in the D-OCT algorithm, after adjusting for confounders, statistically significant differences were observed at OCT-sites with improved treatment responses to laser. Those deemed "laser resistant" had increased vessel diameter compared to "laser responsive" CMs ($p < 0.001$). Subjects "never treated with laser" and those OCT-sites deemed clinically "laser resistant" had significantly greater vessel diameters, on average, compared to control skin ($p < 0.001$ and $p < 0.001$, respectively). Finally, as in the OCT algorithm analysis, OCT-sites deemed "laser responsive" demonstrated no differences in vessel diameter compared to anatomically matched control skin ($p = 0.971$), Table 3. When comparing the OCT device algorithm to this image-generated watershed analysis, an R^2 value of 0.33 was calculated, which equates to a correlation coefficient of 0.57 (23) (Figure S3).

4 | Discussion

Our study further adds to the literature regarding opportunities and limitations of D-OCT to measure key characteristics of vascular networks within PWCMs. The use of both device-generated and open-source water segmentation methods is a methodologic strength in this work, supporting reproducible quantitation of vascular features. In our manuscript, the Michelson Diagnostics' (Maidstone, England) proprietary D-OCT algorithm measurements demonstrated "moderate" correlation with the open-sourced watershed analysis ($R = 0.57$), suggesting that the device algorithm provides a reasonable proxy for vessel diameter.

Limitations of this work include the small sample size, including those who consented to next-generation sequencing for molecular diagnosis. In addition, artifact was noted in a subset of images due to motion, precluding analysis across all images. Our study aligns with previous literature, which demonstrates that D-OCT can non-invasively characterize vascular morphology and dynamics in PWCMs, and that quantitative imaging metrics can reveal clinically relevant heterogeneity. Previous studies have demonstrated statistically significant differences in affected PWCMs and anatomically matched control skin, by lesional location on the body, and by vascular plexus depth as a function of color [24–26]. Our findings corroborate this previous work, demonstrating statistically significant differences between the vasculature of PWCMs and normal skin, and by PWCM location.

Larger diameter vessels in GNAQ variant PWCMs are hypothesized to result from upregulation of the vascular growth factor, angiopoietin-2 [29]. Qualitatively, we observed that patients with "low-flow" variant PWCMs harbored larger diameter vessels, on average, on D-OCT, in comparison to both

10969101, 0, Downloaded from https://onlinelibrary.wiley.com/doi/10.1002/lsm.70223 by University Of California Irvine Science Library Serials, Wiley Online Library on [06/11/2026]. See the Terms and Conditions (https://onlinelibrary.wiley.com/terms-and-conditions) on Wiley Online Library for rules of use; OA articles are governed by the applicable Creative Commons License

TABLE 2 | Vessel Diameter based on D-OCT Algorithm. Differences in vessel diameter utilizing D-OCT by "low-flow" vs. "fast-flow" genotype (GNAQ/GNA11 vs. EPHB4/RASA1), location, age, and treatment response, using D-OCT algorithm. Control skin is defined by anatomically matched, unaffected skin (on the contralateral side). Responsive to treatment is classified as ≥ 70% clinical clearance of the lesion.

			Univariable analysis				Multivariable analysis*		
Variable	**Level**	***N*^**	**Mean (95% CI)**	**ANOVA *p*-value**	**Post-hoc Contrasts**	**Post-hoc Adjusted *p*-value**	**ANOVA *p***	**Post-hoc contrasts**	**Post-hoc adjusted *p*-value**
Age, range	< 2	38	0.102 (0.062, 0.142)	0.587			0.515		
	2–18	68	0.106 (0.085, 0.127)						
	19–39	30	0.116 (0.081, 0.151)						
	≥ 40	37	0.081 (0.041, 0.121)						
Genotype flow	Control	44	0.069 (0.050, 0.088)	< 0.001	C vs. LF	< 0.001	< 0.001	C vs. LF	< 0.001
	Low-flow	72	0.135 (0.113, 0.158)		C vs. Unk	0.027		C vs. Unk	0.040
	Fast-flow	9	0.121 (0.079, 0.163)						
	Unknown	48	0.105 (0.083, 0.128)						
Affected	Control	44	0.068 (0.049, 0.087)	[#]< 0.001			[#]< 0.001		
	Affected	129	0.121 (0.105, 0.136)						
Location	Head/Neck	153	0.112 (0.096, 0.128)	[#]0.033	H/N vs. Limbs	0.034	[#]0.080		
	Trunk	8	0.086 (0.034, 0.138)						
	Limbs	12	0.052 (0.007, 0.096)						
Response to treatment	Control	44	0.068 (0.051, 0.084)	[#]< 0.001	C vs. UnT	[#]0.001	[#]< 0.001	C vs. UnT	[#]0.001
	Untreated	27	0.119 (0.096, 0.142)		C vs. LResist	[#]< 0.001		C vs. LResist	[#]< 0.001
	LResist	35	0.174 (0.153, 0.195)		UnT vs. LResist	[#]0.002		UnT vs. LResist	[#]0.008
	LResp	67	0.083 (0.065, 0.101)		UnT vs. LResp	[#]0.039		UnT vs. LResp	[#]0.030
					LResist vs. LResp	[#]< 0.001		LResist vs. LResp	[#]< 0.001

Abbreviations: C, control; FF, fast flow (EPHB4 and RASA1); H/N, head/neck; LF, low flow (GNAQ and GNA11); LResist, laser resistant (< 70% clearance clinically); LResp, laser responsive (> 70% clearance clinically); Unk, unknown; UnT, untreated.

^*N* is number of PWCMs in each level. Mean (95% CI) as estimated by univariable mixed effects ANOVA with lesion and matched control pair as a random effect.

*Multivariable analysis controls for Age and number of previous laser treatments.

[#]Notes statistically significant values.

10969101, 0, Downloaded from https://onlinelibrary.wiley.com/doi/10.1002/lsm.70223 by University Of California Irvine Science Library Serials, Wiley Online Library on [06/11/2026]. See the Terms and Conditions (https://onlinelibrary.wiley.com/terms-and-conditions) on Wiley Online Library for rules of use; OA articles are governed by the applicable Creative Commons License

TABLE 3 | Vessel areas (surrogate for vessel diameter) based on watershed analysis. Differences in vessel areas calculated by watershed analysis utilizing D-OCT by genotype (Low-Flow vs. Fast-Flow), location, age, and treatment response. Control skin is defined by anatomically matched, unaffected skin (on the contralateral side). Responsive to treatment is classified as ≥ 70% clinical clearance of the lesion.

							Multivariable analysis*		
Variable	**Level**	***N*^**	**Mean (95% CI)**	**ANOVA *p*-value**	**Post-hoc contrasts**	**Post-hoc adjusted *p*-value**	**ANOVA *p***	**Post-hoc contrasts**	**Post-hoc adjusted *p*-value**
Age, range	< 2	38	0.024 (0.020, 0.029)	0.707			0.803		
	2–18	68	0.025 (0.023, 0.027)						
	19–39	30	0.023 (0.019, 0.027)						
	≥ 40	76	0.023 (0.019, 0.027)						
Genotype flow	Control	46	0.021 (0.019, 0.023)	#< 0.001	C vs. LF	< 0.001	#< 0.001	C vs. LF	#0.007
	Low-flow	109	0.026 (0.023, 0.028)		C vs. FF	0.003		C vs. FF	#0.009
	Fast-flow	9	0.029 (0.024, 0.033)		C vs. Unk	0.031		C vs. Unk	#0.033
	Unknown	48	0.025 (0.022, 0.027)						
Affected	Control	46	0.021 (0.019, 0.023)	<# 0.001			#< 0.001		
	Affected	166	0.026 (0.024, 0.027)						
Location	Head/Neck	190	0.026 (0.025, 0.027)	#< 0.001	H/N vs. Limbs	< 0.001	#< 0.001	H/N vs. Limbs	#< 0.001
	Trunk	8	0.020 (0.016, 0.025)						
	Limbs	14	0.015 (0.011, 0.018)						
Response to treatment	Control	46	0.021 (0.019, 0.023)	#< 0.001	C vs. UnT	#0.001	#< 0.001	C vs. UnT	#< 0.001
	Untreated	27	0.026 (0.023, 0.028)		C vs. LResist	#< 0.001		C vs. LResist	#< 0.001
	LResist	72	0.030 (0.028, 0.032)		UnT vs. LResist	#0.011		UnT vs. LResist	#0.015
	LResp	67	0.021 (0.019, 0.023)		UnT vs. LResp	#0.002		UnT vs. LResp	#0.001
					LResist vs. LResp	#< 0.001		LResist vs. LResp	#< 0.001

Abbreviations: C, control; FF, fast flow; H/N, head/neck; LF, low flow; LResist, laser resistant (< 70% clearance clinically); LResp, laser responsive (> 70% clearance clinically); Unk, unknown; UnT, untreated.
^*N* is the number of PWCMs in each level. Mean (95% CI) as estimated by univariable mixed effects ANOVA with lesion and matched control pair as a random effect.
*Multivariable analysis controls for Age and the number of previous laser treatments.
#Notes statistically significant values.

10969101, 0, Downloaded from https://onlinelibrary.wiley.com/doi/10.1002/lsm.70223 by University Of California Irvine Science Library Serials, Wiley Online Library on [06/11/2026]. See the Terms and Conditions (https://onlinelibrary.wiley.com/terms-and-conditions) on Wiley Online Library for rules of use; OA articles are governed by the applicable Creative Commons License

anatomically matched control skin and in patients with "fast-flow" variants (Figure 1). However, across each 6×6 mm image, these findings were not statistically significant. The small sample size of genotyped patients is a limitation that could confound statistical significance. However, the high degree of vessel heterogeneity might also be explained by low variant allele frequency, as GNAQ and GNA11 variants occurred in $< 5\%$ of affected cells in our population (range 2.2%–4.7%). This might explain why many of the vessels within each imaged area were of normal caliber. Based on our data, both by D-OCT algorithm and watershed segmentation, we suspect that the relatively small proportion of larger-diameter (likely aberrant) vessels is obfuscated by a larger proportion of smaller, surrounding vessels. The superficial depth of OCT resolution may also limit the evaluation of deeper vessels harboring the variant. At least in our small sample size, this data suggests significant heterogeneity within PWCM images and underscores that D-OCT did not show significant genotype discrimination in this cohort.

When stratified by age, we found no observable differences in measurement using either the D-OCT algorithm or watershed analysis. This stands in contrast to previous biopsy studies, which have demonstrated statistically significant differences in vessel size on histopathology, with more dilated vessels noted in older patients [1, 7, 18]. Small sample size could contribute to our findings, but limitations in D-OCT likely also confound the analysis. These limitations include the superficial depth of resolution, precluding commentary regarding deeper vessels, and dependence on measurement of flow, particularly in the extremities, where gravity would be anticipated to reduce flow.

Importantly, statistically significant differences were observed between vessels at OCT-imaged sites in CMs with excellent laser responses, compared to those never treated with laser, or with poor responses to laser ("laser resistance"), even after adjusting for potential confounders, including the number of laser treatments and age at initiation of laser. Because this study was cross-sectional, with enrollment of patients across the life spectrum, OCT was not performed prior to every treatment with laser in all cases; however, 48% of patients were imaged prior to initiation of the first-ever laser. Within this cohort, vessel diameters were found to increase in those who were poorly responsive to treatment, with statistical significance < 0.001 using both the OCT algorithm and Watershed analysis. This could result from the inability of the laser to completely photocoagulate larger diameter vessels, although the findings remain associative rather than causative. Laser does alter the cutaneous vasculature, and therefore, prospective studies with initiation of OCT prior to any laser treatment would be most critical to confirm these findings, and to determine if D-OCT can be utilized to improve laser-treatment planning based on vessel characteristics. For example, with vessels of increased diameter, longer pulse durations might be required with "pulse stacking" to provide better efficacy in these patients.

5 | Conclusion

By linking D-OCT–derived vascular metrics with treatment responses, this work corroborates previous studies suggesting that vessel characteristics contribute to laser outcomes. In this preliminary cohort, D-OCT did not discriminate genotypes but showed a strong association with laser treatment responses. These findings suggest that D-OCT-derived vessel diameter might serve as a non-invasive predictor of treatment outcome. Prospective studies with larger samples and standardized treatment protocols are needed to confirm clinical utility. Generative AI was not used in the creation of this study or the data generated in this manuscript.

Acknowledgments

Christina Sheehan, Hannah Kolarik, Chandra Singh. We are grateful for funding support from the Dermatology Foundation (Arkin CDA), Sturge Weber Foundation, the Pediatric Dermatology Research Alliance, University of Wisconsin ICTR, University of Wisconsin Skin Disease Research Center, NIH P41 GM135019 (KWE). We acknowledge the intellectual and technical contributions of Scott Hetzel of the Biostatistics and Epidemiology Research Design Core to the development of this manuscript. This work was funded by the Institutional Clinical and Translational Science Award UL1 TR002373." Michelson Diagnostics provided the use of equipment to UC-Irvine.

Ethics Statement

Reviewed and approved by University of Wisconsin IRB; approval #472920.

Consent

Consent for the publication of recognizable patient photographs or other identifiable material was obtained by the authors and included at the time of article submission to the journal, stating that all patients gave consent with the understanding that this information may be publicly available.

Conflicts of Interest

B.D.: Cofounder, Board of Directors, and Owner of Arkayli Biopharma, Board of Directors, Isthmus Project. K.K.: Equipment: Lutronic, Michelson Diagnostics, Sciton, Cutera; Consultant: Shanghai Fudan-Zhangjiang Biopharmaceutical, Candela, Sciton, Primus Pharmaceuticals. L.A.: Amgen, Eli Lily (PI: funds to the institution), Eli Lily (Consulting, not relevant to this work). The other authors declare no conflicts of interest.

Data Availability Statement

The data that support the findings of this study are available in the supplementary material of this article.

References

1. D. C. Goldenberg, M. Vikkula, A. Penington, et al., "Updated Classification of Vascular Anomalies. A Living Document From the International Society for the Study of Vascular Anomalies Classification Group," *Journal of Vascular Anomalies* 6 (2025): e113.

2. A. M. Hammill and E. Boscolo, "Capillary Malformations," *Journal of Clinical Investigation* 134, no. 8 (2024): e172842. https://doi.org/10.1172/JCI172842.

3. M. D. Shirley, H. Tang, C. J. Gallione, et al., "Sturge-Weber Syndrome and Port-Wine Stains Caused by Somatic Mutation in GNAQ," *New England Journal of Medicine* 368 (2013): 1971–1979.

4. D. Zhang, L. F. Sánchez-Espino, M. Ivars, et al., "Phenotypic Spectrum of GNA11 R183C Mosaicism," *Pediatric Dermatology* 42 (2025): 475–480.

10969101, 0, Downloaded from https://onlinelibrary.wiley.com/doi/10.1002/lsm.70223 by University Of California Irvine Science Library Serials, Wiley Online Library on [06/11/2026]. See the Terms and Conditions (https://onlinelibrary.wiley.com/terms-and-conditions) on Wiley Online Library for rules of use; OA articles are governed by the applicable Creative Commons License

5. M. Wassef, F. Blei, D. Adams, et al., "Vascular Anomalies Classification: Recommendations From the International Society for the Study of Vascular Anomalies," *Pediatrics* 136 (2015): e203–e214.

6. M. De Bortoli, A. Queisser, V. C. Pham, et al., "Somatic Loss-Of-Function PIK3R1 and Activating Non-Hotspot PIK3CA Mutations Associated With Capillary Malformation With Dilated Veins (CMDV)," *Journal of Investigative Dermatology* 144 (2024): 2066–2077.e6.

7. L. M. Boon, J. B. Mulliken, and M. Vikkula, "RASA1: Variable Phenotype With Capillary and Arteriovenous Malformations," *Current Opinion in Genetics & Development* 15 (2005): 265–269.

8. Y. Sun, L. Su, Y. Zhang, et al., "Genotype–Phenotype and Genotype–Outcome Analysis of Capillary Malformation–Arteriovenous Malformation," *Journal of Vascular Anomalies* 4 (2023): e052.

9. R. Waelchli, S. E. Aylett, K. Robinson, W. K. Chong, A. E. Martinez, and V. A. Kinsler, "New Vascular Classification of Port-Wine Stains: Improving Prediction of Sturge-Weber Risk," *British Journal of Dermatology* 171 (2014): 861–867.

10. N. Revencu, L. M. Boon, A. Mendola, et al., "RASA1 Mutations and Associated Phenotypes in 68 Families With Capillary Malformation-Arteriovenous Malformation," *Human Mutation* 34 (2013): 1632–1641.

11. R. W. Ten Broek, A. Eijkelenboom, C. J. M. van der Vleuten, et al., "Comprehensive Molecular and Clinicopathological Analysis of Vascular Malformations: A Study of 319 Cases," *Genes, Chromosomes and Cancer* 58 (2019): 541–550.

12. S. E. Wetzel-Strong, F. Galeffi, C. Benavides, et al., "Developmental Expression of the Sturge-Weber Syndrome-Associated Genetic Mutation in Gnaq: A Formal Test of Happle's Paradominant Inheritance Hypothesis," *Genetics* 224, no. 4 (2023): iyad077. https://doi.org/10.1093/genetics/iyad077.

13. D. H. Siegel, C. E. Cottrell, J. L. Streicher, et al., "Analyzing the Genetic Spectrum of Vascular Anomalies With Overgrowth via Cancer Genomics," *Journal of Investigative Dermatology* 138 (2018): 957–967.

14. R. R. Anderson and J. A. Parrish, "Selective Photothermolysis: Precise Microsurgery by Selective Absorption of Pulsed Radiation," *Science* 220 (1983): 524–527.

15. R. G. Geronemus and R. Ashinoff, "The Medical Necessity of Evaluation and Treatment of Port-Wine Stains," *Journal of Dermatologic Surgery and Oncology* 17 (1991): 76–79.

16. S. L. Hagen, K. R. Grey, D. Z. Korta, and K. M. Kelly, "Quality of Life in Adults With Facial Port-Wine Stains," *Journal of the American Academy of Dermatology* 76 (2017): 695–702.

17. E. J. Fiskerstrand, L. O. Svaasand, G. Kopstad, K. Ryggen, and S. Aase, "Photothermally Induced Vessel-Wall Necrosis After Pulsed Dye Laser Treatment: Lack of Response in Port-Wine Stains With Small Sized or Deeply Located Vessels," *Journal of Investigative Dermatology* 107 (1996): 671–675.

18. E. J. Fiskerstrand, L. O. Svaasand, G. Kopstad, M. Dalaker, L. T. Norvang, and G. Volden, "Laser Treatment of Port Wine Stains: Therapeutic Outcome in Relation to Morphological Parameters," *British Journal of Dermatology* 134 (1996): 1039–1043.

19. H. Jeon, L. J. Bernstein, D. A. Belkin, S. Ghalili, and R. G. Geronemus, "Pulsed Dye Laser Treatment of Port-Wine Stains in Infancy Without the Need for General Anesthesia," *JAMA Dermatology* 155 (2019): 435–441.

20. S. Bajaj, J. Tao, D. A. Hashemi, and R. G. Geronemus, "Weekly Pulsed Dye Laser Treatments for Port-Wine Birthmarks in Infants," *JAMA Dermatology* 160 (2024): 606–611.

21. L. Themstrup, J. Welzel, S. Ciardo, et al., "Validation of Dynamic Optical Coherence Tomography for Non-Invasive, In Vivo Microcirculation Imaging of the Skin," *Microvascular Research* 107 (2016): 97–105.

22. B. Wan, C. Ganier, X. Du-Harpur, et al., "Applications and Future Directions for Optical Coherence Tomography in Dermatology," *British Journal of Dermatology* 184 (2021): 1014–1022.

23. J. Olsen, J. Holmes, and G. B. E. Jemec, "Advances in Optical Coherence Tomography in Dermatology-A Review," *Journal of Biomedical Optics* 23 (2018): 1–10.

24. J. N. Mehrabi, J. Holmes, M. Abrouk, et al., "Vascular Characteristics of Port Wine Birthmarks as Measured by Dynamic Optical Coherence Tomography," *Journal of the American Academy of Dermatology* 85 (2021): 1537–1543.

25. J. V. Wang, J. N. Mehrabi, M. Abrouk, et al., "Analysis of Port-Wine Birthmark Vascular Characteristics by Location: Utility of Optical Coherence Tomography Mapping," *Lasers in Surgery and Medicine* 54 (2022): 98–104.

26. J. S. Waibel, J. Holmes, A. Rudnick, D. Woods, and K. M. Kelly, "Angiographic Optical Coherence Tomography Imaging of Hemangiomas and Port Wine Birthmarks," *Lasers in Surgery and Medicine* 50 (2018): 718–726.

27. R. A. Elsanadi, F. Messele, J. Lee, B. Choi, and K. M. Kelly, "Optical Coherence Tomography-Measured Blood Vessel Characteristics of Port-Wine Birthmarks by Depth: A Cross-Sectional Study," *Journal of the American Academy of Dermatology* 91 (2024): 848–854.

28. J. Schindelin, I. Arganda-Carreras, E. Frise, et al., "Fiji: An Open-Source Platform for Biological-Image Analysis," *Nature Methods* 9 (2012): 676–682.

29. L. Huang, C. Bichsel, A. L. Norris, et al., "Endothelial GNAQ p.R183Q Increases ANGPT2 (Angiopoietin-2) and Drives Formation of Enlarged Blood Vessels," *Arteriosclerosis, Thrombosis, and Vascular Biology* 42 (2022): e27–e43.

Supporting Information

Additional supporting information can be found online in the Supporting Information section.

Supporting File 1: lsm70223-sup-0001-Supplemental_Figure_1.tiff.
Supporting File 2: lsm70223-sup-0002-Supplemental_Figure_2.tiff.
Supporting File 3: lsm70223-sup-0003-Supplemental_Figure_3.tiff.
Supporting File 4: lsm70223-sup-0004-Supplemental_Table_1.tiff.

10969101, 0, Downloaded from https://onlinelibrary.wiley.com/doi/10.1002/lsm.70223 by University Of California Irvine Science Library Serials, Wiley Online Library on [06/11/2026]. See the Terms and Conditions (https://onlinelibrary.wiley.com/terms-and-conditions) on Wiley Online Library for rules of use; OA articles are governed by the applicable Creative Commons License